Elena Lazzeri • Alberto Si
Paola Anna Erba • Napole
Giovanni D'Errico • Giulia

Radionuclide
of Infection
and Inflamm

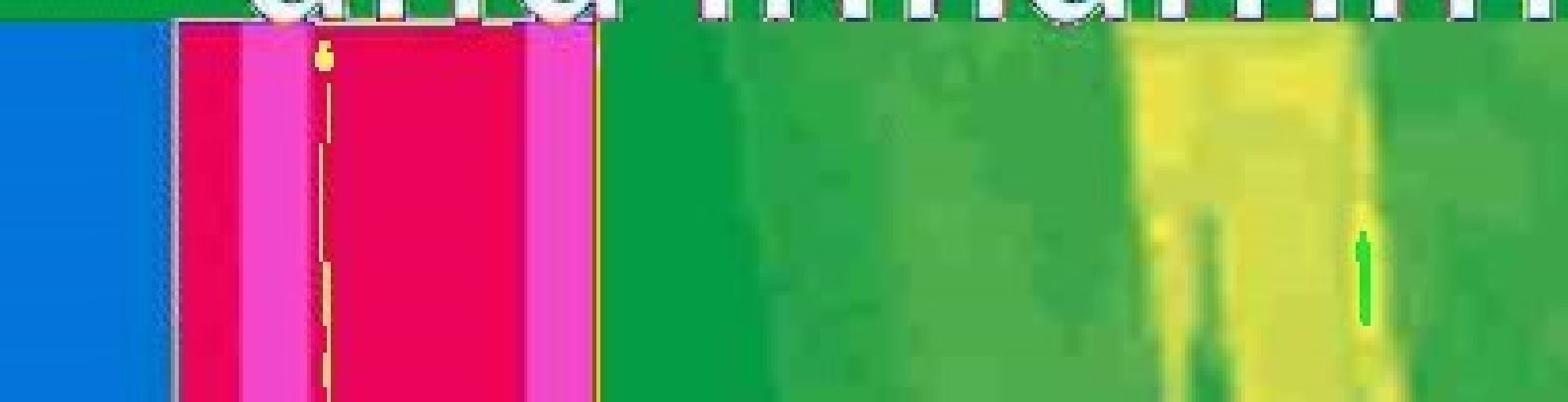

Radionuclide Imaging of Infection and Inflammation

Elena Lazzeri • Alberto Signore
Paola Anna Erba • Napoleone Prandini
Annibale Versari • Giovanni D'Errico
Giuliano Mariani

Radionuclide Imaging of Infection and Inflammation

A Pictorial Case-Based Atlas

Forewords by Christopher J. Palestro
and Giovanni Lucignani

Springer

Elena Lazzeri
Regional Center of Nuclear Medicine
University of Pisa Medical School
Pisa, Italy

Alberto Signore
Nuclear Medicine, Department of Surgery
and Translational Medicine
University of Rome "La Sapienza", S. Andrea Hospital
Rome, Italy

Paola Anna Erba
Regional Center of Nuclear Medicine
University of Pisa Medical School
Pisa, Italy

Napoleone Prandini
Nuclear Medicine Department
Policlinico di Modena
Modena, Italy

Annibale Versari
Nuclear Medicine
Santa Maria Nuova Hospital IRCCS
Reggio Emilia, Italy

Giovanni D'Errico
Nuclear Medicine Department
Private Hospital "Pio XI"
Rome, Italy

Giuliano Mariani
Regional Center of Nuclear Medicine
University of Pisa Medical School
Pisa, Italy

ISBN 978-88-470-2762-6 ISBN 978-88-470-2763-3 (eBook)
DOI 10.1007/978-88-470-2763-3
Springer Milan Dordrecht Heidelberg London New York

Library of Congress Control Number: 2012950699

7 6 5 4 3 2 1 2013 2014 2015
Cover design: Ikona S.r.l., Milan, Italy
Typesetting: Grafiche Porpora S.r.l., Segrate (MI), Italy

Springer-Verlag Italia S.r.l. – Via Decembrio 28 – I-20137 Milan
Springer is a part of Springer Science+Business Media (www.springer.com)

Foreword

There have been significant advances in our understanding of microorganisms and the pathogenesis of infection and inflammation as well as an increased availability of antimicrobial therapy in recent decades. Infection, nevertheless, remains a major cause of patient morbidity and mortality throughout the world. While the presence of infection may be suggested by certain signs and symptoms such as pain, loss of appetite, fever, general malaise and abnormal laboratory results, imaging studies often are used to localize or confirm the presence of infection. The imaging studies can be divided into two principal categories: morphological and functional. Morphological, or anatomic, imaging tests, such as radiographs, ultrasound, computed tomography and magnetic resonance, reveal anatomic or structural alterations in tissues or organs, which, in infection, are caused by a combination of microbial invasion and the immune response of the host to the invasion. Functional imaging studies, which are typified by radionuclide tests, make use of small quantities of radioactive material, or tracers that either are taken up by cells, tissues and organs directly, or are attached to native substances that subsequently migrate to the region of interest. Radiolabeled bisphosphonates, for example, are directly incorporated into the bone. Radiopharmaceuticals labeled with indium-111 or technetium-99m bind intracellularly in leukocytes, and are therefore used to monitor white cell accumulation at foci of infection. Other functional imaging tests used for localizing infection include gallium-67 citrate (and more recently the positron emitter gallium-68), and [^{18}F]fluorodeoxyglucose positron emission tomography ([^{18}F]FDG-PET).

Although radionuclide imaging has been used for diagnosing and localizing infection for nearly fifty years, and despite significant advances in agents, equipment, and imaging techniques, “nuclear infectology” has often been overshadowed by other areas of our specialty. One only has to compare the plethora of texts devoted to radionuclide imaging in oncology with the very few devoted to inflammation and infection in order to appreciate the void in our specialty.

Merely publishing a textbook, however, does not ensure its quality. Textbooks, regardless of whether they are of the traditional print or the more recent e-book style, are the foundation of medical knowledge, providing basic facts and a broad overview of a topic. The best textbooks do not contain exhaustive detail, or subtleties of diagnosis or management, all of which can be found in complementary resources. The success and value of a textbook depends on the organization, accessibility, and substantiality, of the information within.

Radionuclide Imaging of Infection and Inflammation: A Pictorial Case-Based Atlas edited by Lazzeri, Signore, Erba, Prandini, Versari, D’Errico and Mariani, admirably fulfills the criteria of the successful textbook. It begins with a thorough review of the commonly used radiopharmaceuticals, including the normal biodistributions, variants and pitfalls in image interpretation. This information not only sets the stage, and is especially useful, for studying the chapters that follow, but also provides the reader a readily accessible section for reference, when questions in other chapters, and even in daily practice, arise. The role of nuclear medicine in the usual clinical scenarios, such as soft tissue and musculoskeletal infections as

well as in fever of unknown origin (FUO), is thoroughly covered, objectively presented, well illustrated and referenced. Equally important are the chapters devoted to somewhat less well known or at least less frequently reviewed, situations such as infections of the lungs, central nervous system, and cardiovascular implantable devices, as well as chronic inflammatory diseases. The clinical cases provided at the end of the chapters provide valuable teaching points to supplement and enhance the text. The illustrations have been thoughtfully chosen and carefully prepared, incorporating the latest in hybrid imaging techniques.

It is gratifying indeed that this atlas has been organized by clinical entity rather than by technology. Our primary focus, albeit through imaging, is that of patient care, and it is both logical and better for the patient and for us, to focus on diseases rather than on technologies.

I now invite you, my fellow student, to read, to enjoy, and especially, to learn from *Radionuclide Imaging of Infection and Inflammation: A Pictorial Case-Based Atlas.*

October 2012

Christopher J. Palestro, M.D.
Professor of Radiology
Hofstra North Shore - Long Island Jewish School of Medicine
Hempstead, New York

Chief of Nuclear Medicine & Molecular Imaging
North Shore Long Island Jewish Health System
Manhasset & New Hyde Park, New York

Foreword

The publication of this Atlas is an important achievement for the "Infection and Inflammation" Study Group of the Italian Association of Nuclear Medicine (AIMN), not least because it will allow the group's expertise to be shared with colleagues worldwide. It is also a tangible reflection of the high level of professionalism and cooperation that exists within the group.

The fact that it is published by Springer will certainly help the AIMN in its pursuit of a key aim: to promote the efficient dissemination of scientific data and advances in the field of nuclear medicine that have relevance to other disciplines. In this regard, this Atlas follows in the footsteps of other publications produced within the context of the Italian nuclear medicine community.

As current president of the AIMN, I am therefore delighted by the completion of this volume, which will undoubtedly strengthen our knowledge of diagnostic nuclear medicine.

October 2012

Giovanni Lucignani
President of the Italian Association
of Nuclear Medicine (AIMN)

Preface

Inflammation is the physiological response of the body to any injury, which may be constituted by infection, a simple trauma, reduced blood supply, or also a tumor. The inflammatory response involves endothelial/vascular changes, local production of several chemotactic factors and cytokines, migration and accumulation of different types of immune cells (the task of which is to repair tissue damage and/or to destroy infectious agents), and postinflammatory events (such as granulomas or fibrosis). The pattern of immune cell population and the resulting histopathologic features differ according to the type of injury and its persistence over time. When inflammation is elicited in response to infection, granulocytes are continuously recruited by chemotactic bacterial factors; in trauma and degenerative diseases, granulocytes may be present transiently, but are followed by a lymphocytic infiltration; in the presence of tumor cells, NK cells and macrophages predominate; in autoimmune diseases and graft rejection, it is T- and B-cells in addition to macrophages that predominate. If the pathological injury persists over time, inflammation may further evolve from an 'acute' type reaction to a 'chronic' type reaction, which is generally characterized by a lesser degree of vascular involvement and more important mononuclear cell infiltration, with eventual formation of granulomas or fibrosis.

All such features are not highly specific for any particular type of injury, and may in fact have various overlaps, both in terms of type of cell population involved and in terms of time-related patterns. Therefore, the inflammatory response should be considered as a 'dynamic' process self-adapting to an evolving pathophysiologic condition, rather than a 'stereotyped' response elicited indifferently by all injuries.

Diagnostic imaging with modern molecular nuclear medicine is based on the availability of sensitive and relatively specific radiopharmaceuticals tailored for the different targets that can be expressed in this complex scenario.

Three important consequences emerge from the above considerations: i) choice of the 'best' radiopharmaceutical for imaging infection/inflammation should be based on clinical ground, as well as on the timing and etiology of the process; ii) dynamic pathophysiology of the inflammatory process (with its associated histopathologic features) is the basis for distinguishing a 'sterile acute inflammation' from a 'septic acute inflammation', or a 'sterile chronic inflammation' from a 'septic chronic inflammation'; iii) correct diagnosis of infection/inflammation is dictated by optimal use of the available radiopharmaceuticals (in terms of indication for employing a particular imaging agent and in terms of preparation and quality control), as well as by optimal use of image acquisition protocols, image elaboration, and image interpretation.

Throughout this atlas the term 'inflammation' is frequently used as synonymous with 'sterile acute inflammation' or 'sterile chronic inflammation', while the term 'infection' is used as a synonym of 'septic acute inflammation' or 'septic chronic inflammation'.

While several radiopharmaceuticals are now commercially available for imaging infection, many others are currently under investigation, including radiolabeled cytokines, peptides, some monoclonal antibodies, antibiotics, vitamins, etc. This atlas only deals with the routine clinical use of commercially available radiopharmaceuticals or cell preparations, such as radiolabelled leukocytes (^{99m}Tc-HMPAO and ^{111}In-oxine), nanocolloids, monoclonal antibodies, ^{67}Ga-citrate and [^{18}F]FDG.

We refer the reader to other textbooks and guidelines for thorough, in-depth understanding of the use of available radiopharmaceuticals, indications, acquisition protocols, and interpretation criteria. Whereas, the goal of this atlas is to guide the practitioners and students through a wide selection of diagnostic images as obtained in the clinical routine of different centers for different clinical conditions involving infection/inflammation. We placed special emphasis on information enabling the recognition of the normal biodistribution patterns of radiopharmaceuticals (including possible pitfalls and artifacts, as discussed in Chapter 1), as well as the main imaging findings in more than 30 different inflammatory/infective disorders.

Some chapters describe the most frequent infection/inflammation conditions that are referred to nuclear medicine departments for diagnosis and characterization, such as bone and joint infection (Chapters 3 and 11), joint prosthesis infections (Chapter 4), vascular prosthesis infection (Chapter 5), fever of unknown origin (Chapter 9), and inflammatory bowel diseases (Chapter 10). All such chapters include some teaching cases, where it is quite easy (also for the untrained eye) to recognize, even on planar imaging, the abnormal accumulation of radiopharmaceutical over time at the site of infection, while in some other cases the comparison between planar and tomographic images emphasizes the added value of hybrid imaging (mostly SPECT/CT) to exactly localize the site of infection and its extension to surrounding structures.

Other chapters describe less common diseases, that are therefore illustrated with fewer diagnostic cases, such as soft tissue infections (Chapter 2), infection of non-orthopedic prosthesis implants and resident electronic medical devices (Chapter 6), infections of the central nervous system and head and neck structures (Chapter 7), infective endocarditis (Chapter 8), lung infections (Chapter 12), and inflammatory, noninfectious diseases such as vasculitis, sarcoidosis, rheumatoid arthritis, etc. (Chapter 13). The scans included in these chapters have been selected so as to indicate how, in the evaluation of some cases such as infective endocarditis or chest vascular prosthesis, SPECT/CT imaging is an essential requirement for correct diagnostic interpretation.

With this atlas we intended to fill an important gap in the nuclear medicine books published so far, by providing the essential background both for understanding the pathophysiologic basis of radionuclide imaging of infection/inflammation and for correctly interpreting the diagnostic images obtained in these conditions. Nevertheless, the role of nuclear medicine imaging in each condition is presented in the general perspective commonly encountered in the clinical practice, which also includes the use of other imaging modalities. The ‘clinical cases’ have the purpose of demonstrating the clinical impact of nuclear medicine imaging procedures in the workout of patients with suspected infection/inflammation.

This atlas is the result of years of common work with colleagues of the Study Group of Inflammation/Infection of the Italian Association of Nuclear Medicine (AIMN). All authors have contributed both by writing specific chapters and by providing images and clinical cases for all chapters. Not only the authors, but also many other colleagues from Italy and from abroad have contributed interesting pictures and clinical cases. We are therefore deeply indebted to all such contributors, who are acknowledged at the end of each chapter. In particular, our close collaborators, Dr Roberto Boni, Dr Marta Pacilio, Dr Virginia Rossetti, and Dr Martina Sollini deserve special acknowledgements.

Last but not least, we wish to thank the team of publishers at Springer for allowing us to prepare and publish this atlas book in a very short time.

October 2012

Elena Lazzeri
Alberto Signore
Paola Anna Erba
Napoleone Prandini
Annibale Versari
Giovanni D’Errico
Giuliano Mariani

Contents

Contributors

Fausto Beretta Service of Diabetology, Dietetics and Clinical Nutrition, Sant'Anna Hospital, Ferrara, Italy

Alberto Biggi Nuclear Medicne, Santa Croce e Carle Hospital, Cuneo, Italia

Roberto Boni Regional Center of Nuclear Medicine, University of Pisa Medical School, Pisa, Italy

Gaetano Caruso Clinical Orthopedics, University of Ferrara, Ferrara, Italy

Giuseppe L. Cascini Nuclear Medicine, University of Catanzaro, Catanzaro, Italy

Giovanni D'Errico Nuclear Medicine Department, Private Hospital "Pio XI", Rome, Italy

Paola Anna Erba Regional Center of Nuclear Medicine, University of Pisa Medical School, Pisa, Italy

Lorenzo Fantini Nuclear Medicine, S.Orsola-Malpighi Hospital, Bologna, Italy

Elena Lazzeri Regional Center of Nuclear Medicine, University of Pisa Medical School, Pisa, Italy

Giuliano Mariani Regional Center of Nuclear Medicine, University of Pisa Medical School, Pisa, Italy

Jose Martin-Comin Diagnostic Imaging Institute (IDI), Hospital University of Bellvitge, IDIBELL, Barcelona, Spain

Giulia Pazzola Rheumatology Unit, Department of Internal Medicine, Azienda Ospedaliera Arcispedale S. Maria Nuova, Reggio Emilia, Italy

Chiara Peterle Nuclear Medicine Unit Department, S. Anna University Hospital of Ferrara, Italy

Nicolò Pipitone Rheumatology Unit, Department of Internal Medicine, Azienda Ospedaliera Arcispedale S. Maria Nuova, Reggio Emilia, Italy

Napoleone Prandini Nuclear Medicine Department, Policlinico di Modena, Modena, Italy

Ilaria Rambaldi Nuclear Medicine Unit Department, S. Anna University Hospital of Ferrara, Italy

Carlo Salvarani Rheumatology Unit, Department of Internal Medicine, Azienda Ospedaliera Arcispedale S. Maria Nuova, Reggio Emilia, Italy

Alberto Signore Nuclear Medicine, Department of Surgery and Translational Medicine, University of Rome "La Sapienza", S. Andrea Hospital, Rome, Italy

Martina Sollini Nuclear Medicine, Azienda Ospedaliera Arcispedale S. Maria Nuova, Reggio Emilia, Italy

Annibale Versari Nuclear Medicine, Santa Maria Nuova Hospital IRCCS, Reggio Emilia, Italy

1 Normal Findings from Different Radiopharmaceuticals and Techniques, with Variants and Pitfalls

Annibale Versari

The pharmacokinetic and/or pharmacodynamic pattern of radiopharmaceuticals in patients may be affected by several factors including a variety of drugs, disease states and, in some cases, surgical procedure [1]. Among the factors that can change radiopharmaceutical biodistribution, co-administration of interfering drugs is the most commonly reported occurrence [2]. Drug-radiopharmaceutical interactions may arise as a result of the mode of drug action, of physico-chemical interactions between drugs and radiotracers, and of competition for common binding sites [2–4]. Table 1.1 lists drugs that can interfere with the biodistribution of ^{67}Ga-citrate, radiolabeled leukocytes and [^{18}F]FDG in patients [5].

Also faulty radiopharmaceutical preparation (including contamination during dispensing or administration, and errors in the labeling procedure for ^{111}In-oxine or ^{99m}Tc-HMPAO-leukocytes) may alter the subsequent biodistribution of radiopharmaceuticals, thus affecting the diagnostic quality of scintigraphic images [3, 6–12]. Although less commonly, radiopharmaceuticals may also interact with the syringe's or intravenous line components [13, 14]. Also some lifestyle factors, such as smoking, alcohol intake and dietary habits (i.e., high-dose vitamins) have the potential of interacting with radiopharmaceuticals [15]. Additionally, the use of monoclonal antibodies of murine origin may induce the generation of human antimouse antibodies (HAMA), which can lead to allergic reactions and altered pharmacokinetics upon repeated injections [16].

Finally, technical pitfalls that may affect the results of imaging include equipment-related artifacts (i.e., inadequate quality-control procedures/calibration), image processing-related artifacts (i.e., misregistration of the CT component with the SPECT or PET component), patient-related artifacts (i.e., patient motion) [6] and radiopharmaceutical extravasation during administration [6, 17, 18] (Fig. 1.1).

Tables 1.2 and 1.3 summarize the main physiological characteristics and distribution of radiopharmaceuticals discussed in this chapter [16].

1.1 ^{67}Ga-citrate Scintigraphy

1.1.1 Normal Biodistribution

About 10%–25% of the injected activity is excreted through the kidneys during the first 24 hours after administration, after which the principal route of excretion is the large bowel. By 48 hours after injection, about 75% of the injected activity remaining in the body is equally distributed among the liver, bone/bone marrow, and soft tissues. Typical whole-body and spot images acquired at 24 and 72 hours post-injection of ^{67}Ga-citrate are shown in Figs. 1.2 and 1.3. ^{67}Ga-citrate localizes in bone marrow because it is incorporated as an iron analogue into the forming red blood cells; some (low degree) localization in bone is due to the $^{67}Ga^{2+}$ ion weakly mimicking distribution of the calcium ions. Localization in the nasopharynx, lacrimal glands, salivary, thymus, breasts, spleen and genitalia is variable [19–21].

1.1.2 Normal Variants

1. Below 2 years of age, increased thymic activity is common [22].
2. Hilar lymph node localization (usually low-grade) can be seen in adult patients, particularly in smokers [23].
3. Increased breast activity, which is otherwise generally faint and symmetric, although it can be more intense in hy-

A. Versari (✉)
Nuclear Medicine
Santa Maria Nuova Hospital IRCCS
Reggio Emilia, Italy
e-mail: versari.annibale@asmn.re.it

E. Lazzeri et al., *Radionuclide Imaging of Infection and Inflammation*,
DOI 10.1007/978-88-470-2763-3_1

Table 1.1 Drugs that can interfere with biodistribution of the radiopharmaceuticals/procedures most commonly employed for imaging inflammatory and infectious diseases (adapted from AIMN procedural Guide-Lines: http://www.aimn.it/pubblicazioni/LG/RP_AIMN_infezioni.pdf)

Radiopharmaceutical/Preparation	Pharmaceutical Class	Drug
^{67}Ga-citrate	Mineral supplements	Iron
		Calcium gluconate (parenteral)
	Chemotherapeutics	All
	Steroids	Prednisolon
Radiolabeled leukocytes	Beta lactam antibiotics	Cephalosporin
	Immunosuppressive	Azathioprine
		Cyclophosphamide
	Steroids	Prednisolone
	Calcium-antagonists	Nifedipine
	Anticoagulant	Heparin
	Sulphamide	Sulfasalazine
	Iron	Iron
[^{18}F]FDG	Steroids	Prednisolone
	Antiepileptics	Valproate
		Carbamazepine
		Phenytoin
		Phenobarbital
	Catecholamines	Catecholamines

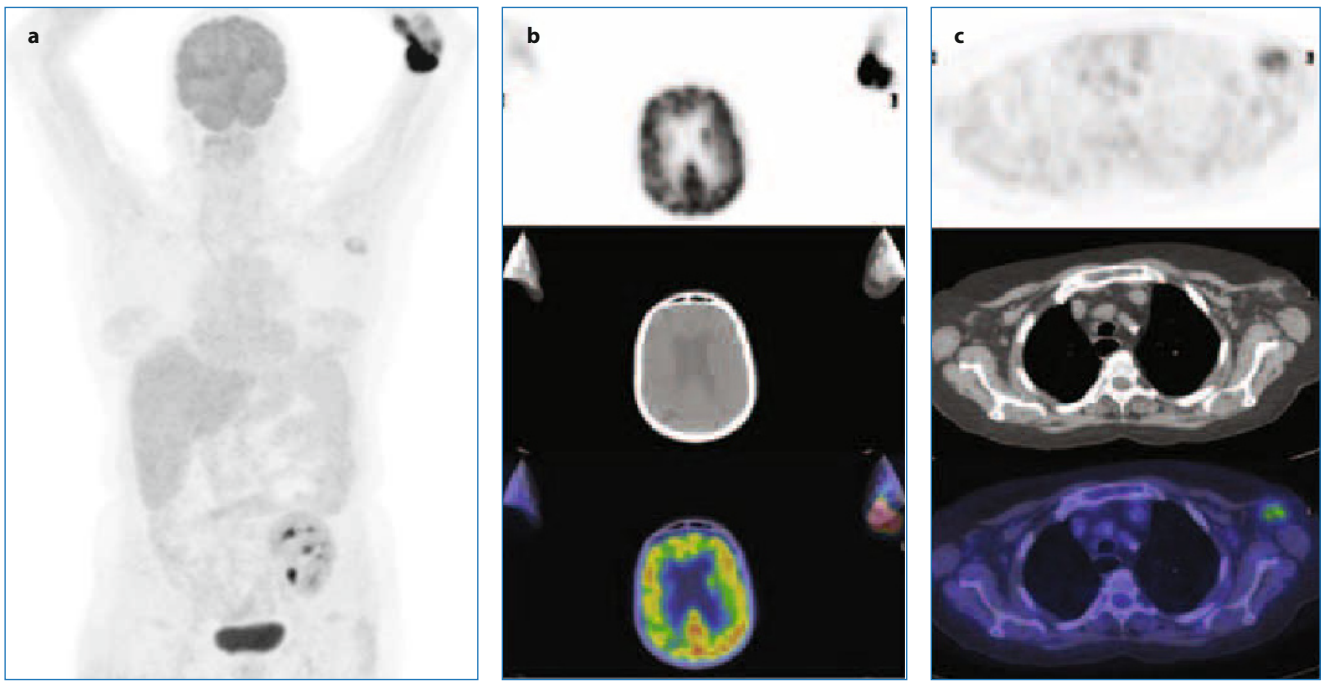

Fig. 1.1 MIP [^{18}F]FDG-PET/CT image (**a**) shows intense radiopharmaceutical localization at injection site (left arm) as confirmed by transaxial views (**b**) (PET, *upper image*; CT, *middle*, fused, *lower*) associated with mild uptake in the left axilla (**c**) due to lymphatic drainage after [^{18}F]FDG extravasation during administration

Table 1.2 Targeting mechanisms of the radiopharmaceuticals most commonly employed for imaging inflammatory/infectious disease (modified from Laverman P et al. Current Radiopharmaceuticals, 2008, Vol. 1, No. 1)

Physiological characteristics	Targeting mechanism	Radiopharmaceutical/Preparation
Enhanced vascular permeability	Transferrin and lactoferrin receptor binding	^{67}Ga-citrate
Enhanced vascular permeability and increased bone metabolism	Adsorption on hydroxyapatite crystals	^{99m}Tc-methylene diphosphonate (MDP)
Enhanced vascular permeability and endothelial activation	Uptake in activated endothelial cells	^{99m}Tc-sulfur colloid
Enhanced vascular permeability and chemiotactic activation	Chemiotactic activation	Radiolabeled leukocytes
Enhanced vascular permeability and cell-binding	Antigen binding	^{99m}Tc-anti-NCA-95 IgG, BW 250/183, besilesomab (Scintimun®)
		^{99m}Tc-anti-SSEA-1 IgM, falonesomab (Leu-Tech®, NutroSpec®)
		^{99m}Tc-anti-NCA-90 Fab', sulesomab (LeukoScan®)
Increased metabolic requirements	Enhanced glucose uptake in activated cells	[^{18}F]FDG

Table 1.3 Physiologic whole-body distribution of the radiopharmaceuticals most commonly used for imaging inflammatory/infectious disease (modified from Becker W. The contribution of nuclear medicine to the patient with infection. Eur J Nucl Med 1995)

Radiopharmaceutical	Liver	Spleen	Kidney	Bladder	Bowel	Bone		Blood
						Cortical	Marrow	
^{67}Ga-citrate	Yes	Yes	Yes	Yes	Yes	No	Yes	No
^{99m}Tc-MDP/HDP	No	No	Yes	Yes	No	Yes	No	No
^{99m}Tc-nanocolloids	Yes	Yes	Yes	Yes	No	No	Yes	No
^{111}In-oxine-leukocyte	Yes	Yes	No	No	No	No	Yes	No
^{99m}Tc-HMPAO-leukocytes	Yes	Yes	Yes	Yes	Yes	No	Yes	No
^{99m}Tc-anti-granulocyte Ab	Yes	Yes	Yes	Yes	No	No	Yes	No
[^{18}F]FDG	Yes	Yes	Yes	Yes	No	No	No	No

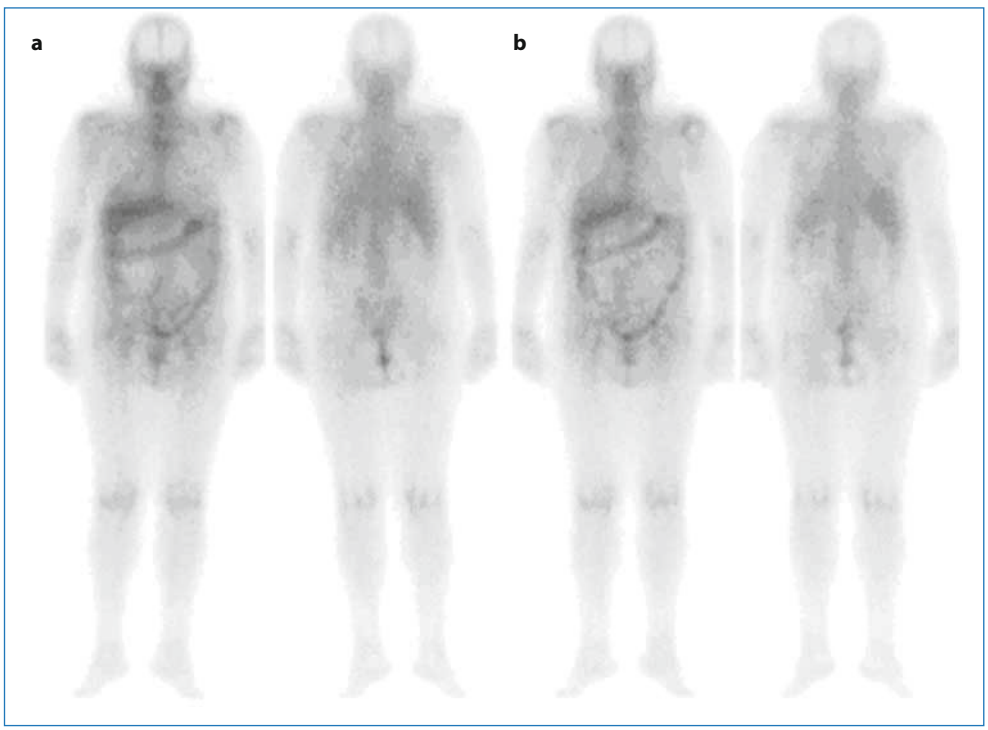

Fig. 1.2 ^{67}Ga-citrate scintigraphy: whole body images (*left* and *right*) in anterior and posterior views obtained 48 hours (**a**) and 72 hours (**b**) after i.v. administration, showing normal biodistribution in the liver, bone and bone marrow, and soft tissues 48 hours after injection. Similar pattern of distribution at 72 hours. Both images show radiopharmaceutical localization in the large bowel (principal route of excretion from 24 hours post-injection onward)

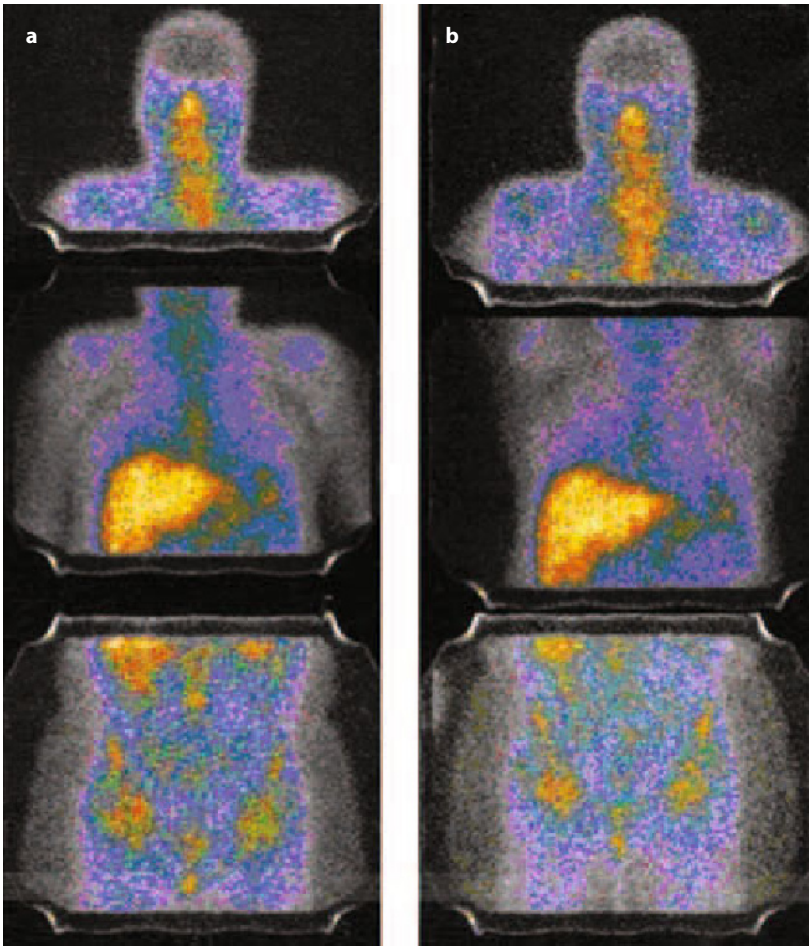

Fig. 1.3 Normal ^{67}Ga-citrate scintigraphy: anterior spot views of the head/neck (*upper panels*), chest (*middle panels*) and abdomen (*lower panels*) obtained 48 hours (**a**) and 72 hours (**b**) post-injection. Physiologic soft tissue visualization, with relatively intense radiopharmaceutical uptake in the liver (*middle panels*) and mild localization in pelvic bone/bone marrow (*lower panels*). Moderate radiopharmaceutical localization in the nasopharynx can also be seen (*upper panels*)

perprolactinemia (associated physiologically with pregnancy and lactation, but possibly caused by numerous drugs, renal failure, in addition to prolactin-producing pituitary adenomas or to hypothalamic lesions which determine interruption of the hypothalamic-pituitary axis) [24, 25].

1.1.3 Pitfalls

1. Residual bowel activity is probably the most common cause for both false-positive and false-negative interpretations [26].
2. In children and teenagers, increased activity can be seen in the case of thymic hyperplasia, secondary to chemotherapy [27].
3. Gadolinium administered for MRI enhancement within 24 hours before the ^{67}Ga-citrate injection, has been reported to decrease localization of the radiopharmaceutical [28].
4. Saturation of iron-binding transferrin sites (i.e., hemolysis or multiple blood transfusions) causes altered gallium-67 distribution resulting in increased renal, bladder, and bone activities and in reduced liver uptake and reduced accumulation in the colon [19].
5. Gallium-67 uptake at sites of bone repair, secondary to healing fractures or prior orthopedic hardware sites, loose prostheses, or after successful treatment of osteomyelitis, may complicate interpretation in patients with suspected osteomyelitis [29].
6. Recent chemotherapy and external beam radiation therapy [26].
7. Recent surgical wounds can induce increased radiopharmaceutical uptake, persisting up to 2 weeks after the event [29].
8. Uptake at cutaneous metal retention sutures, due to reaction at the site of insertion or other skin contact [29].
9. Desferoxamine therapy increases renal excretion of the tracer and enhances target-to-background ratios [30].
10. Hilar, submandibular and diffuse pulmonary radiopharmaceutical localization in patients with lymphoma during therapy [20].
11. Radiation sialadenitis causes increased localization [31].
12. Possible uptake in a variety of tumors (i.e., lymphoma, lung cancer, mesothelioma, melanoma) [20, 32–36].
13. Physiologic liver uptake may be decreased in patients with AIDS or acute lymphocytic leukemia [26].
14. Diffusely increased pulmonary activity can occur in a

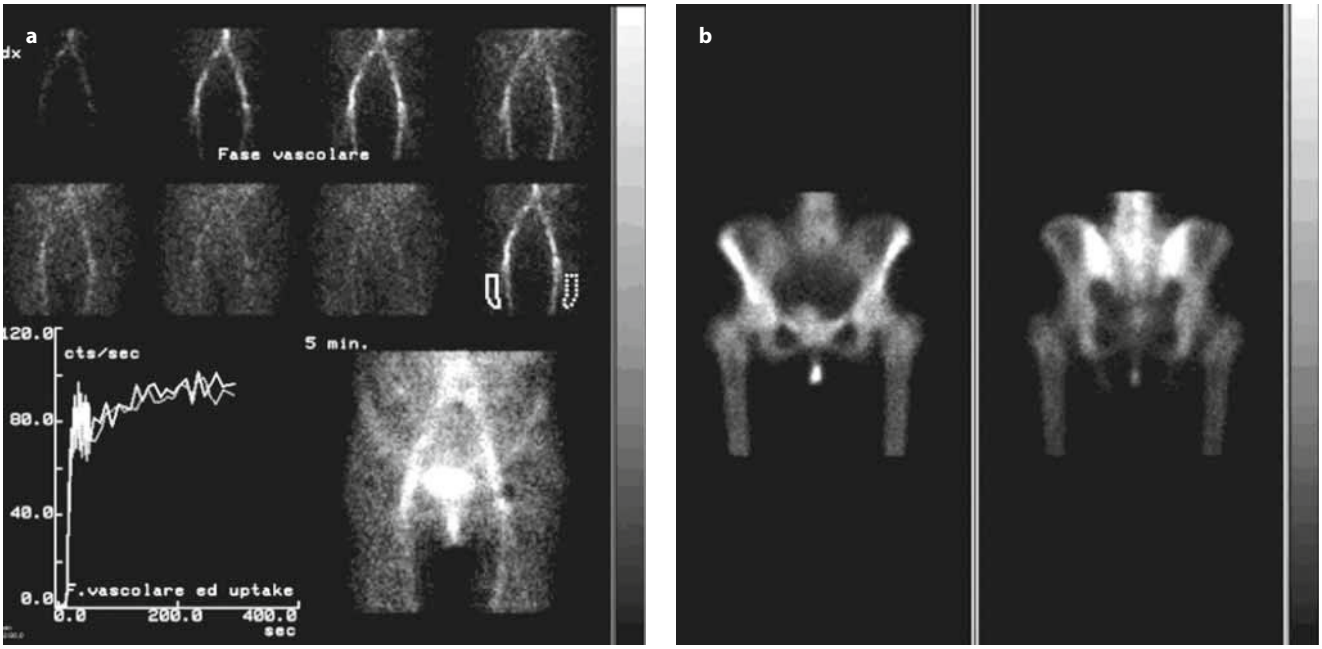

Fig. 1.4 ^{99m}Tc-MDP three-phase scintigraphy of the hip. (**a**) Arrival of the radiopharmaceutical in the region of interest; by drawing regions of interest (ROIs) on the suspected site of altered vascularization and on the corresponding contralateral, supposedly healthy site, it is possible to calculate time-activity curves. (**b**) Delayed scintigraphic acquisition (anterior and posterior images, *left* and *right*) obtained 3 hours p.i., showing normal uptake of the pelvic bones

variety of non-infectious diseases as in cases of sarcoidosis, idiopathic pulmonary fibrosis, lymphoid interstitial pneumonitis, hypersensitivity pneumonitis, talc-induced granulomatosis, inhalational/occupational pulmonary diseases (asbestosis, berylliosis, coal worker pneumoconiosis, and silicosis), collagen vascular diseases (systemic lupus erythematosus and systemic sclerosis), eosinophilic pneumonia, multicentric reticulohistiocytosis, Wegener's granulomatosis, eosinophilic granuloma, drug toxicity (amiodarone, bleomycin, procarbazine, cyclophosphamide, nitrofurantoin, tocainide, busulfan) and reaction to iodinated contrast material (lipiodol) [37–61].

1.2 ^{99m}Tc-diphosphonate (MDP/HDP) Scintigraphy

1.2.1 Normal Biodistribution

Excretion occurs primarily through the renal route. Up to 70% of the injected activity being excreted within 6 hours post-injection. Radiopharmaceutical uptake depends on local blood flow, osteoblastic activity, and extraction efficiency [6]. In a normal adult subject, the bone scan shows a higher concentration of activity in some parts of the skeleton, as in the spine (trabecular bone with large mineralizing bone surface), compared with the shafts of long bones (predominantly cortical bone) [62–67]. Renal and urinary bladder activities are normally present at the time of acquisition (about 3 hours post-injection for a conventional bone scan) and minimal soft-tissue activity is usually observed [6] (Fig. 1.4). This normal pattern of distribution, however, is subject to considerable variation. In patients with significantly impaired renal function, the scans may be delayed to allow better clearance of extra-cellular fluid and vascular activity [66, 68].

1.2.2 Normal Variants

1. Increased uptake at the confluence of sutures in the skull; such uptake can be more pronounced in patients with metabolic bone disease, such as renal osteodystrophy [65].
2. In elderly patients increased uptake in the skull can be observed (especially in the frontal region and calvarium, due to hyperostosis frontalis interna) because of thickening of the frontal bones; such uptake can be more pronounced following chemotherapy in cancer patients, or in cases of metabolic bone disease [64].
3. Symmetrical or asymmetrical focal photopenia can be present in the parietal region, due to thinning of the parietal bone compared to the remaining portions of the skull [64].
4. Increased uptake at the manubrio-sternal junction [6].
5. A small photopenic defect (sternal foramina) surrounded by uniformly distributed radioactivity uptake can be

observed in the inferior part of the sternum, due to the incomplete fusion of the cartilaginous bars in the distal sternum [64].
6. A vertical linear area of increased uptake can be seen distally to the sternum, due to benign tracer uptake in the xiphisternum [6].
7. A focal area of increased uptake can be noted in the proximal/mid humeri at the site of insertion of skeletal muscles at the deltoid tuberosity [6].
8. Increased uptake in the pubic symphysis and possibly in the sacroiliac joints can be observed in women post-partum, as a consequence of increased stress reaction/pelvic diastases [64].
9. Diffuse breast uptake in women, especially if lactating [6].

1.2.3 Pitfalls

1. Focally increased uptake in the mandible and/or maxillary bone is often due to underlying benign dental pathology [6].
2. Increased tracer uptake in the sinuses is frequently due to infection/inflammatory disease [6].
3. Hypertrophic pulmonary osteoarthropathy typically appears as symmetrically increased uptake of radiotracer in the cortices ('tram lines'), most often seen in the femora, tibiae, and wrists [6].
4. Decreased uptake in the presence of prosthesis (i.e., breast augmentation or orthopedic prosthesis) or of metallic hardware (i.e., cardiac pacemaker), as well as at sites that have previously been included in an external beam radiation field [6].
5. Severe metabolic bone diseases may cause an abnormal radiopharmaceutical biodistribution (i.e., increased uptake at the confluence of head sutures, diffuse uptake in the calvarium) [64].
6. Symmetrical uptake in the acromioclavicular and/or sternoclavicular joint can occur as a consequence of degenerative disease [64].
7. Large vertical linear area of increased uptake in the sternum (sternal split) can be seen in patients who have undergone sternotomy [6].
8. A horizontal linear pattern of increased uptake in the vertebral body is typically observed in cases of fracture; however, it is difficult to differentiate fractures due to benign disease, such as osteoporosis, from vertebral fracture due to a malignant condition [6].
9. Increased uptake in the patella (hot patella sign), even if not considered a real pathological sign, can be seen in association with a wide variety of disorders, such as degenerative disease, Paget disease, and osteomyelitis [64, 69, 70].
10. In patients who have undergone recent surgery, such as knee or hip joint replacements, bone scintigraphy may result in false-positive findings [6].
11. Diffuse breast uptake in cases of gynecomastia induced by hormonal therapy in patients with prostate cancer. Focal breast uptake can be observed in other conditions, both benign and malignant [6].
12. Myocardial uptake can occur in the case of myocardial necrosis/contusion, unstable angina, ventricular aneurysm (focal pattern) or in the case of amyloidosis, hypercalemia, Adriamycin-induced cardiotoxicity, alcoholic cardiomyopathy, pericardial tumors, pericarditis (diffuse pattern) [6].
13. Skeletal muscle uptake can be present in the case of injury/trauma, renal failure, non-traumatic causes (i.e., alcoholic intoxication), scleroderma, polymyositis, carcinomatosis myopathy, muscular dystrophy, dermatomyositis, heterotopic bone formation/myositis ossificans (i.e., following direct trauma, complicated hip arthroplasty) [6].
14. Increased renal uptake can be observed after chemotherapy (vincristine, doxorubicin, cyclophosphamide) or in patients with nephrocalcinosis/hypercalcemia, iron overload, sickle cell disease, acute tubular necrosis (early stages), glomerulonephritis (diffuse pattern) and in the presence of obstructed collecting systems (focal pattern) [6].
15. Decreased renal uptake or non-visualization of the kidneys is generally observed as a consequence of nephrectomy, or in malignant/metabolic superscan. In cases of renal cyst, abscess, tumor, scarring, as well as of partial nephrectomy, a focal area of reduced uptake can be observed [6].
16. Lung uptake can be observed in the case of radiation pneumonitis, hyperparathyroidism/hypocalcemia and, rarely, sarcoidosis [6].
17. Splenic uptake can be present in the case of sickle cell disease, glucose-6-phosphatase deficiency, lymphoma, leukemia, thalassemia [6].
18. Gastric uptake can be observed secondary to hypercalcemia with metastatic calcifications [6].
19. Bowel uptake can be observed in patients with surgical diversion, necrotising enterocolitis or ischemic bowel infarction [6].
20. Liver uptake can occur in the presence of amyloidosis and hepatic necrosis [6].
21. Soft tissue uptake can be observed in a variety of tumors (neuroblastoma, lung/liver tumors/metastases, breast tumors, sarcomas, malignant ascites/pleural effusion) [6].
22. Uptake in calcifications of the major arteries can occur (i.e., femoral artery) [6].
23. Uptake can be seen in areas of cerebral infarct [6].

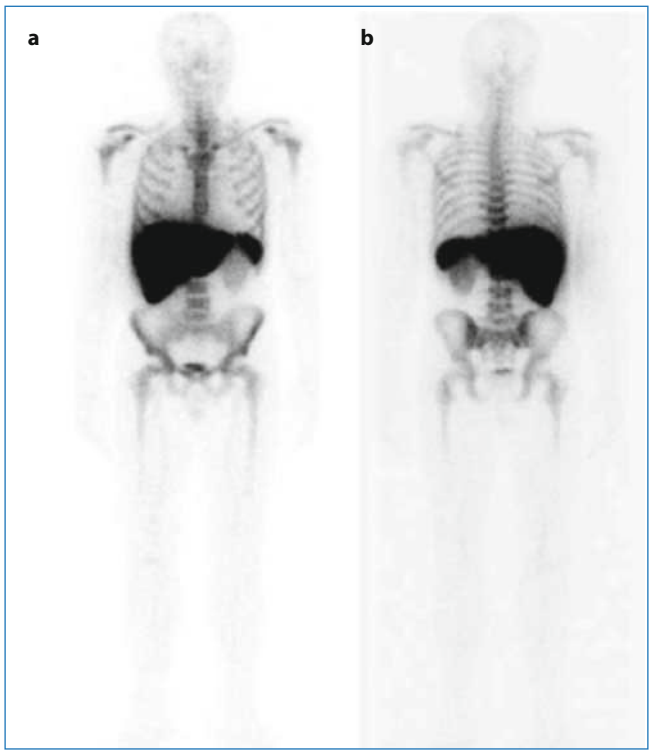

Fig. 1.5 Whole body scan following i.v. administration of ^{99m}Tc-nanocolloids: anterior (**a**) and posterior (**b**) views show predominant uptake in the liver and spleen, with diffuse visualization of active bone marrow

1.3 ^{99m}Tc-nanocolloids

1.3.1 Normal Biodistribution

Following intravenous administration, the injected activity is rapidly cleared from the blood by the reticuloendothelial system (within approximately 2–4 hours). About 55% of the radiopharmaceutical is actively taken up by the reticuloendothelial system, degraded in the lysosomes of macrophages and excreted by the kidney within 24 hours. On average, 80%–90% of the injected particles are phagocytized by the Kupffer cells of the liver; 5%–10% by macrophages in the spleen, and the remaining balance by macrophages in the bone marrow (see Fig. 1.5 for normal pattern of distribution as depicted in a whole body scan). However, uptake of the radiocolloid by the reticuloendothelial system is affected by relative blood flow rates at the various sites, by the functional capacity of the phagocytic cells, and by distribution of hematopoietically active marrow [21, 73].

1.3.2 Pitfalls

Increase bone marrow uptake can be observed in case of aplastic anemia, myeloproliferative disease, and metastasis from solid tumors [71, 72].

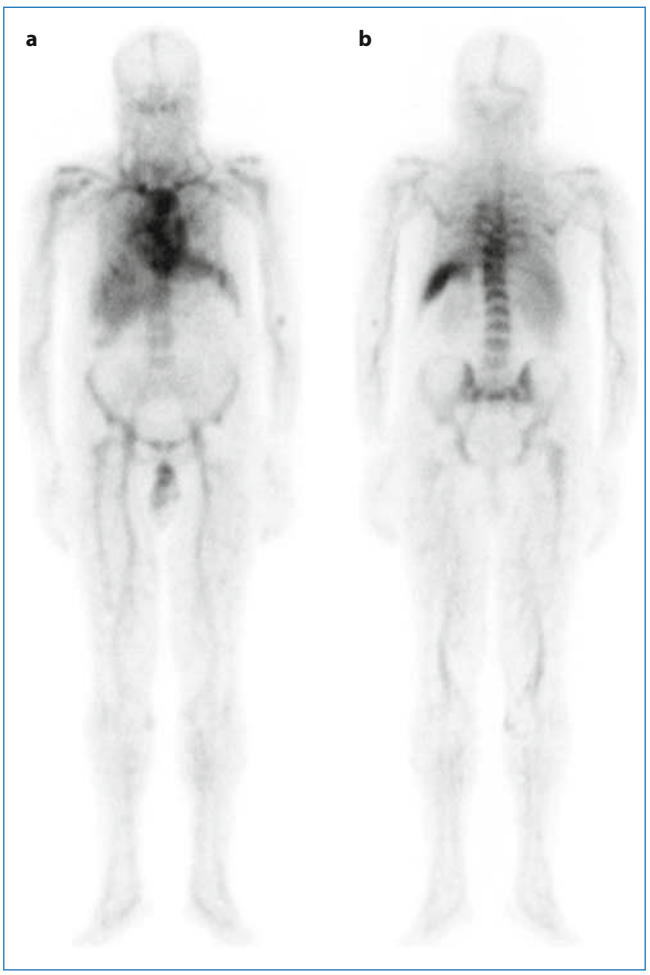

Fig. 1.6 ^{99m}Tc-Scintimun scintigraphy: anterior (**a**) and posterior (**b**) whole body images obtained 30 minutes p.i., showing normal distribution of the radiopharmaceutical with medullary, spleen, liver and blood pool uptake

1.4 ^{99m}Tc-besilesomab BW 250/183 (Scintimun®)

1.4.1 Normal Biodistribution

About 10% of the injected acitivity is bound to neutrophils within 45 minutes post-administration, 20% of the radiopharmaceutical remains free in the circulating blood. Up to 40% of the injected activity accumulates in bone marrow [73, 74] (see example in Fig. 1.6). Spleen, bowel, liver, bone marrow, thyroid and kidney localizations are variable, occurring in up to 6%, to 4%, to 3% and 2% of patients, respectively. This normal distribution pattern is, however, subject to variation.

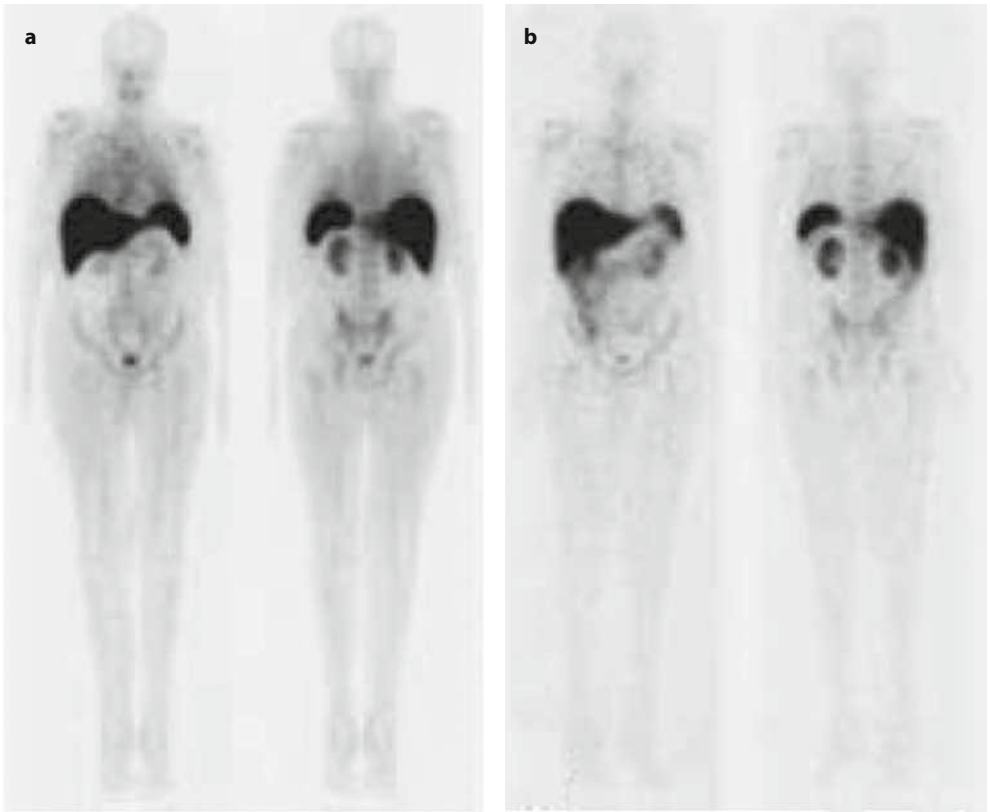

Fig. 1.7 Normal biodistribution of ^{99m}Tc-fanolesomab in anterior and posterior views (*left* and *right*). Images obtained about 2 hours after radiopharmaceutical administration (**a**) show activity within the cardiovascular system, genitourinary tract, liver, spleen, bone marrow and soft tissues. By 24 hours after radiolabeled antigranulocytes mAb (**b**) blood pool activity has cleared and soft tissue activity has diminished thus bone marrow is more prominent and diffuse colonic activity is present. (Copyright from Love C et al. Imaging of infection and inflammation with ^{99m}Tc-fanolesomab. *Q J Nucl Med Mol Imaging* 2006; 50: 113–120)

1.4.2 Pitfalls

1. Due to the physiological uptake in bone marrow, small foci of infection of bone marrow can be obscured [73].
2. Spondylodiscitis and bone metastasis presents 'cold' spots in the scan [75].
3. False positive results can occur in the case of myeloproliferative disease (i.e., multiple myeloma) [76].

1.5 ^{99m}Tc-falonesomab (Leu-Tech®, NeutroSpec®)

1.5.1 Normal Biodistribution

Following intravenous administration, activity is initially distributed in the circulating blood pool. The fraction bound to circulating neutrophils ranges between 11% and 51%, depending on neutrophil count. Bone marrow activity peaks shortly after administration (approximately 14% of injected activity at 2 hours post-administration), with a longer washout time compared to background; the axial and appendicular bone marrow is well visualized. Spleen activity peaks at 5%–12% of the injected amount, 25–30 minutes after injection, falling to about half within 24 hours. Similarly, rapid uptake is seen in the liver, with about 45%–50% of the injected activity 35–65 minutes after administration, decreasing to 25%–40% by 24 hours. There is only minor retention of activity in the lungs [77]. Excretion occurs primarily through the renal route, radioactivity excreted in the urine not being in the form of the intact radiolabeled antibody. Activity excreted through the gastrointestinal tract activity is variable [74, 78–81] (Fig. 1.7).

1.5.2 Pitfalls

Due to physiologic uptake in the bone marrow, small foci of infection of bone marrow can be obscured [73].

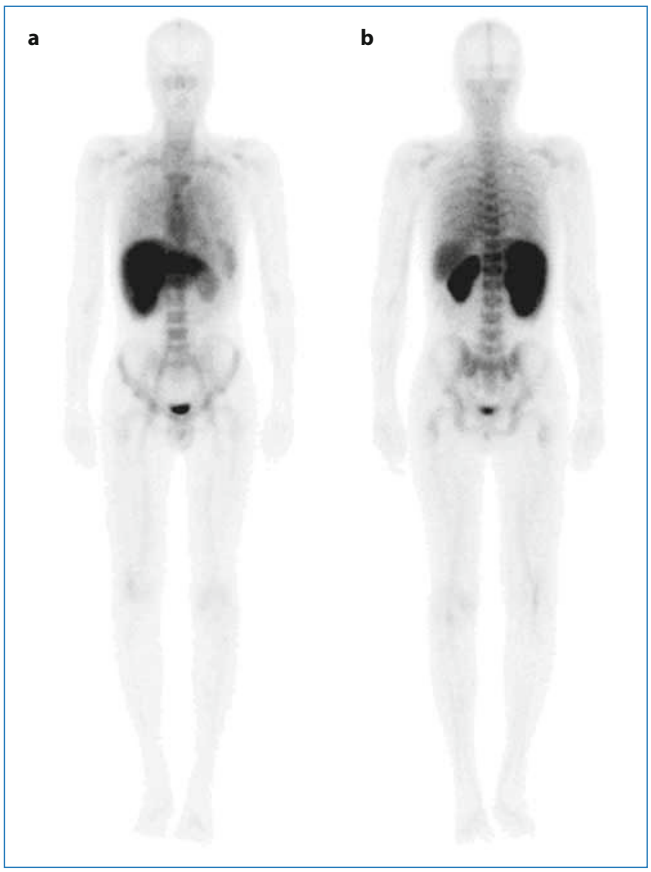

Fig. 1.8 ^{99m}Tc-leukoscan whole body scan: anterior (**a**) and posterior (**b**) views acquired 30 minutes p.i. show a normal pattern of distribution, with uptake in the bone marrow, liver, spleen, and kidneys

1.6 ^{99m}Tc-sulesomab (LeukoScan®)

1.6.1 Normal Biodistribution

About 25%–34% of the injected activity circulates free in the blood, 1 hour after administration, decreasing to 17% at 4 hours and 7% at 24 hours. Activity bound to circulating granulocytes is more than 4% at 1 hour post-injection. Bone marrow activity is about 43% at 1 hour after injection, the remaining activity being distributed in liver, spleen and kidneys (see example in Fig. 1.8). The route of excretion is essentially renal, 41% of the injected activity being recovered in the urine over the first 24 hours post-administration [82, 83].

1.6.2 Pitfalls

1. Due to physiologic uptake in bone marrow small foci of infection of bone marrow can be obscured [73].
2. Spondylodiscitis appears as a 'cold' spot in the scan [84].
3. False-negative results can occur in the presence of orthopedic periprosthetic infection, chronic osteomyelitis (predominance of macrophages and lymphocytes over granulocytes) and abscess with impaired blood perfusion [84, 85].

1.7 ^{111}In-oxine-Leukocyte Scintigraphy

1.7.1 Normal Biodistribution

About 60% of the injected activity is immediately confined to the reticuloendothelial system of the liver, spleen, and bone marrow. There is only a transient migration of labeled cells in the lungs. The radiolabeled cells are cleared exponentially from the circulation, with a half-life between 5 and 10 hours. Final distribution consists of about 20% of the activity in the liver, 25% in the spleen, 30% in the bone marrow, and 25% in other organs. Images acquired up to 4 hours after injection may still show some pulmonary activity (Figs. 1.9 and 1.10). Clearance of activity in liver and spleen is very slow. There is very low excretion of activity in both urine and feces, and no activity is normally observed in the bowel or bladder [86].

1.7.2 Normal Variants

1. Focal uptake can be seen in the presence of an accessory spleen [87].
2. Lymph node activity has been described in children without pathological significance [88, 89].
3. Extramedullary hemopoiesis can result in lymph node activity [90].
4. Though usually solitary, multiple bilateral small round non-segmental lung foci of activity can occur probably due to clumping of cells during the labeling process or during radiopharmaceutical injection complicating interpretation [91, 92].

1.7.3 Pitfalls

1. In the presence of orthopedic hardware or prostheses, normal bone marrow is disrupted and displaced, making the interpretation of ^{111}In-oxine-leukocyte localization in these areas difficult [93].
2. Non-specific bone/joint uptake can occur after bone marrow aspiration or at bone-graft donor sites and in presence of traumatic/degenerative arthritis, gouty arthritis, acute fractures (less than 2 months), traumatic or neuropathic arthropathy, acute bone infarcts, foreign body reaction. Although a rare occurrence, bone neoplasms (i.e., lymphoma with bone involvement) and metastasis, or, active heterotopic bone formation can cause locally increased uptake [94–96].

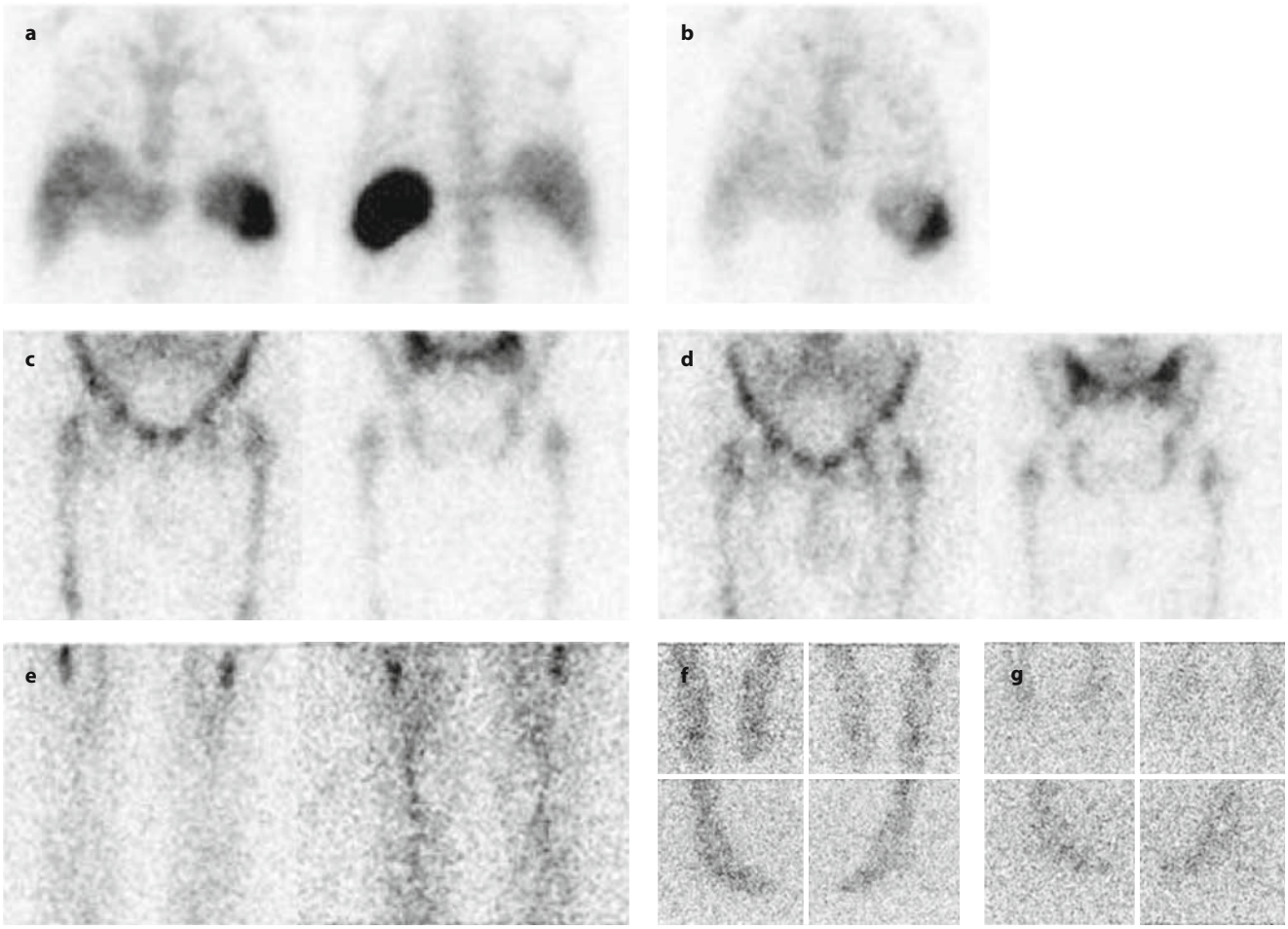

Fig. 1.9 ^{111}In-oxine-leukocyte scintigraphy. Planar spot views of the chest obtained 4 hours (**a**) and 24 hours (**b**) after injection. Early localization in the liver, spleen and bone marrow (**a**), decreasing over time (**b**). Planar anterior and posterior spot views of the pelvis obtained 4 hours (**c**) and 24 hours (**d**) after injection show localization in the bone. Planar anterior and posterior views of the femora (**e**) obtained 24 hours after administration show bone marrow radiolabeled leukocyte uptake at the proximal portion of both femoral diaphyses. Planar spot views of the feet obtained 4 hours (**f**) and 24 hours (**g**) after injection obtained in anterior, posterior (*upper panels*) and lateral views (*lower panels*)

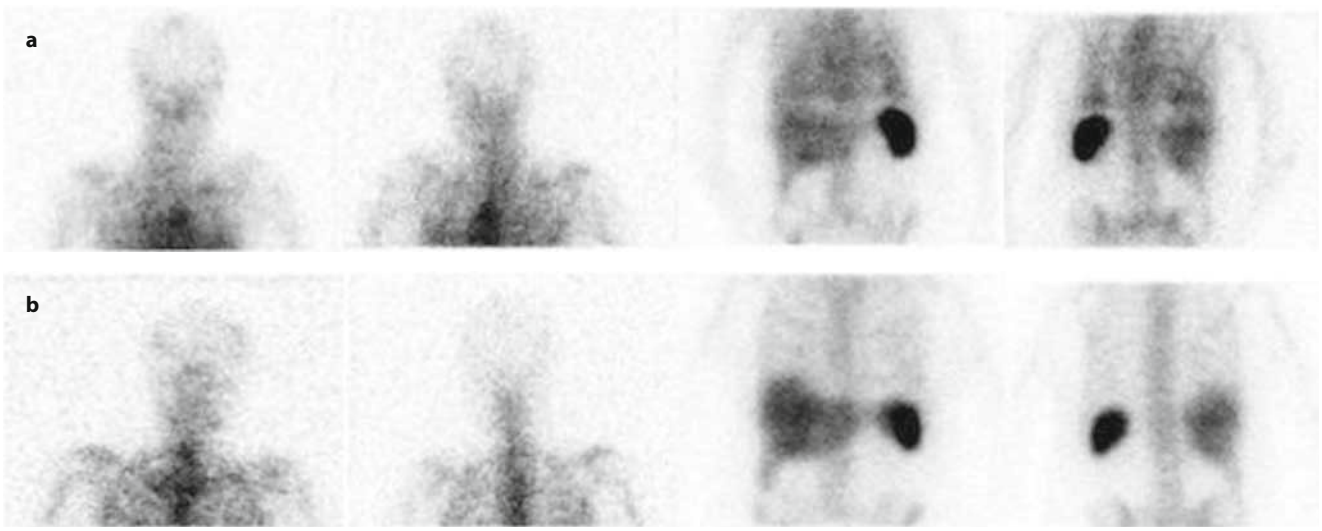

Fig. 1.10 ^{111}In-oxine-leukocyte scintigraphy: planar anterior and posterior spot views of the chest obtained 4 hours (a) and 24 hours (b) after radiolabeled leukocyte injection. Early images (**a**) show multiple bilateral small round non-segmental lung foci of activity due to cell clumping occurring during preparation/administration, a pattern that disappears in the later acquisitions (**b**). Activity in the liver, spleen and bone marrow is also observed

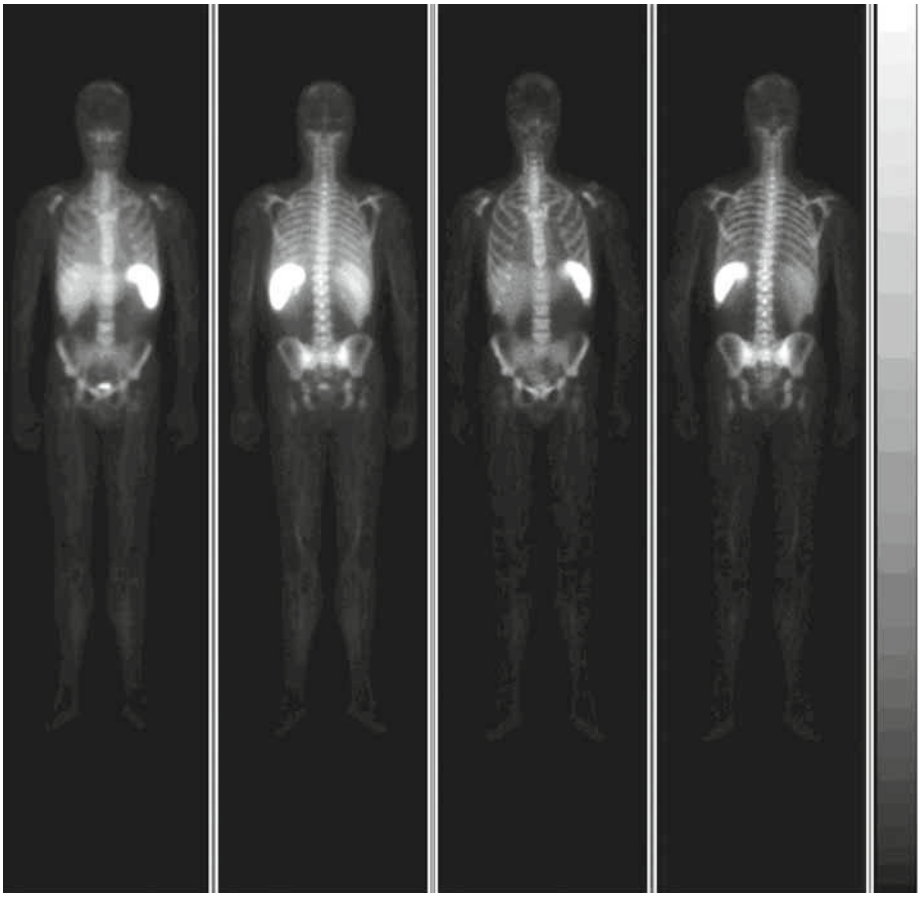

Fig. 1.11 ^{99m}Tc-HMPAO-leukocytes scintigraphy, with different shades of gray: anterior and posterior whole body images (*left* and *right*) acquired 30 minutes p.i., showing physiologic uptake of labeled leukocytes in spleen, liver and bone marrow

3. Prolonged lung uptake can be observed when cells have been damaged during the labeling process.
4. Lung localization can be observed in cystic fibrosis and in patients with adult respiratory distress syndrome [87].
5. Focal uptake can be seen in cases of acute bleedings, hematomas or recent myocardial/cerebral infarcts [21, 87].
6. Uptake can be observed in a variety of tumors (i.e., lymphoma, brain tumors) [93, 97].
7. Diffuse bowel uptake can occur in the presence of non-infectious inflammatory bowel lesion(s) such as stomas, multiple enemas, gastrointestinal bleeding or infarction [8].
8. Chronic walled-off abscesses (more than 3 weeks old), hepatic or splenic abscesses, lymphocytic mediated infection (i.e., granulomatous process, viral infection), low-grade or chronic osteomyelitis (especially in the central skeleton) can be not visualized [98].
9. Abnormally decreased uptake can be seen in severely hypovascular/avascular sites (i.e., cysts, irradiated areas), implants (i.e., prostheses and cardiovascular implantable device) or spondylodiscitis (often appearing as focally decreased uptake compared with adjacent bone marrow) [21, 87, 99–101].
10. External beam radiation therapy induces intense, diffusely increased bone marrow activity at the site of treatment; after treatment, the irradiated sites appear as areas with decreased activity [99, 102].
11. Recent surgical wounds can appear as areas with increased uptake starting at approximately 72 hours, with a complete resolution in a few days. When a surgical wound is not closed, or when it dehisces and is left to heal on its own by secondary intention, uptake persists as an area of intense accumulation even in the absence of infection [21].
12. Non-infected vascular grafts and/or peritoneal shunts can show increased localization because of bleeding or non-infectious reparative process [103].

1.8 ^{99m}Tc-HMPAO-Leukocyte Scintigraphy

1.8.1 Normal Biodistribution

The half life of blood clearance of ^{99m}Tc-HMPAO-leukocytes is about 4 hours. Bowel activity secondary to hepato-biliary secretion of ^{99m}Tc-complexes is usually not seen before 4 hours; physiologic bowel activity is usually faint if seen at 4 hours, and is usually seen in the terminal ileum or right

colon, increasing over time. The pulmonary uptake pattern of labeled leukocytes varies over time. Early images are characterized by diffuse pulmonary activity, which decreases over time; by about 4 hours post-injection, it becomes indistinguishable from background activity (Fig. 1.11). Renal and bladder activities are seen within 15–30 minutes post-injection in patients with normal renal function. Uniform physiologic gallbladder activity can be seen (4% of patients by 2–4 hours and up to 10% of patients by 24 hours). The spleen, liver, bone marrow, kidneys, bowel, bladder, and major blood vessels will normally be visualized [21, 73, 86].

1.8.2 Normal Variants

1. Bowel activity secondary to secretion of ^{99m}Tc-complexes can be detected in 20%–30% of children as early as 1 hour post-injection [104].
2. Though usually solitary, multiple bilateral small round non-segmental lung foci of activity can occur, probably due to clumping of cells during the labeling process or during injection; this occurrence complicates interpretation of the scan [92].
3. Focal uptake can be seen in the presence of accessory spleen(s).

1.8.3 Pitfalls

1. Bone marrow expansion or hyperplasia can alter the normal scintigraphic patterns of bone marrow visualization [21, 100].
2. Lung activity can be present after 3 hours in the case of pulmonary edema, diffuse inflammatory lung disease such as pulmonary drug toxicity (bleomycin, methotrexate, and paclitaxel), atelectasis, radiation pneumonitis, heart or renal failure, sepsis, or adult respiratory distress syndrome or due to cell damage during labeling [20, 86, 105–108].
3. Focal uptake can be seen in the case of neoplasms (i.e., lymphoma, brain tumors) or hematomas [92, 109].
4. Spondilodiscitis may lead to a spot of increased activity or to a 'cold' spot as compared with normal bone marrow localization [21, 110].
5. A 'cold' spot in the spine may occur in the presence of compression fracture, neoplasm, post-irradiation changes, or postsurgical or anatomic deformities [92].
6. Bowel activity (prior to 4 hours) can occur from intraluminal transit of labeled cells secondary to active gastrointestinal bleeding [21].
7. Normal renal activity can make it difficult to detect pyelonephritis and/or renal abscess [104].
8. Chronic walled-off abscesses or low-grade infections, particularly in bone, have reduced accumulation of ^{99m}Tc-granulocytes, and are more likely not to be visualized in the scan [20, 111].
9. Non-infected vascular grafts and/or peritoneal shunts can show increased localization because of bleeding or non-infected reparative process [103].
10. Recent surgical wounds can induce increased uptake by approximately 72 hours, with complete resolution in a few days. When a surgical wound is not closed, or when it dehisces and is left to heal on its own by secondary intention, uptake persists and appears as areas of intense activity even in the absence of infection [21].

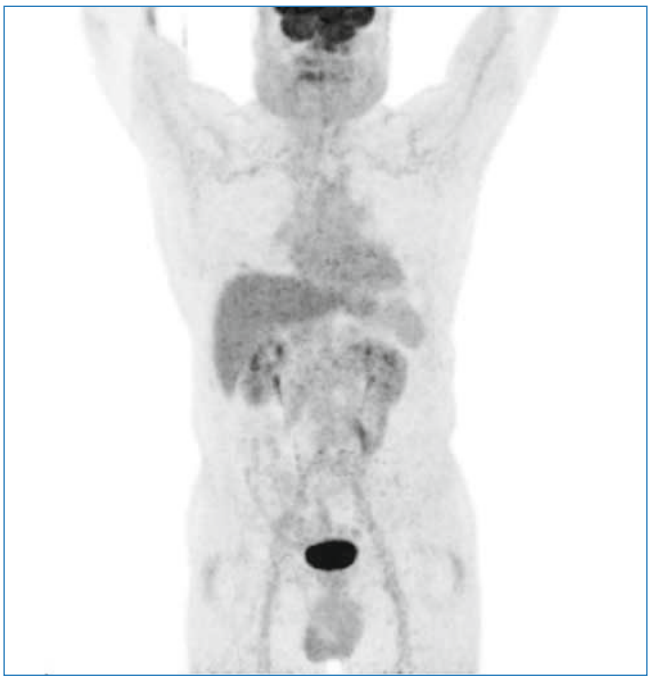

Fig. 1.12 PET/CT MIP image obtained 60 minutes after [^{18}F]FDG injection shows the physiologic pattern of biodistribution of this radiopharmaceutical

1.9 [^{18}F]FDG-PET and [^{18}F]FDG-PET/CT

1.9.1 Normal Biodistribution

[^{18}F]FDG uptake is physiologically most intense in the brain because of predominant glycolytic metabolism in neurons; uptake in the myocardium is variable, since the primary energy source for myocardiocytes is fatty acids. Since [^{18}F]FDG is excreted by the kidney into the urine, intense [^{18}F]FDG activity is normally observed in the intrarenal collecting systems, ureters, and bladder. Even 1 hour after administration, the urinary excretion of [^{18}F]FDG continues in a well-hydrated patient. Less intense and variable physiologic activity is present in the liver, spleen, bone marrow, and renal cortex. At 1 hour post-injection, blood pool activity results in

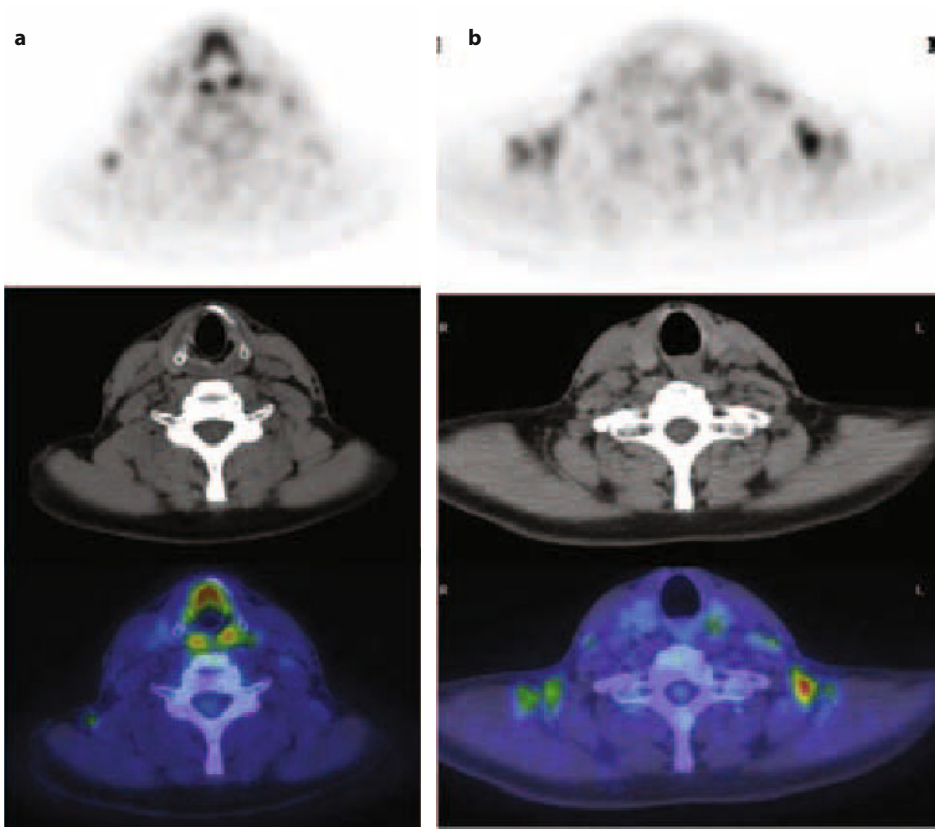

Fig. 1.13 [^{18}F]FDG-PET/CT images (PET images *upper panels*, CT sections *middle panels* and fused PET/CT images *lower panels*) showing two normal variants of [^{18}F]FDG uptake in the same patient. (**a**) [^{18}F]FDG uptake at the epiglottis and arytenoid muscles, due to excessive talking during the time elapsed between tracer injection and scan acquisition. (**b**) Increased uptake in the thermogenic brown fat of the supraclavicular regions (more prominent on the left side in this particular case)

a moderate activity in the mediastinum against a low background lung activity (Fig. 1.12). Uptake in skeletal muscle is generally low if the patient has been allowed sufficient rest after physical activity before tracer injection. The larynx and vocal cords usually show either no uptake or mild symmetric uptake, which may have an inverted U shape [17, 112, 113].

1.9.2 Normal Variants

1. Gastrointestinal activity may have variable intensity and pattern related to multiple factors including muscular peristaltic activity, presence of lymphoid tissue (particularly in the cecum), high concentration of white blood cells in the bowel wall, swallowed secretions, intraluminal concentration of [^{18}F]FDG, colonic microbial uptake, drug interference (i.e., metformin) [114].
2. Intense uptake can be observed in brown adipose tissue, commonly present symmetrically in the midaxillary line, posterior mediastinum, supraclavicular, perihepatic and paraspinal regions [115] (Fig. 1.13).
3. Prominent activity in the laryngeal structures can occur in the case of excessive talking while waiting after tracer injection, before the scan [112] (Fig. 1.13).
4. Cardiac activity is variable, ranging from no discernible activity above background blood pool activity to intense activity throughout the left ventricular myocardium, even in the fasting state [116, 117]. Increased activity can present with a diffuse pattern (with/without heterogeneity), focally (i.e., papillary muscles) or regionally [118] (Fig. 1.14).
5. Physiologic thymic uptake can be observed in childhood, until puberty [119].
6. Mild to moderate uptake is usually seen in the adenoids, in the tonsils, and at the base of the tongue in children, due to the physiologic activity of lymphatic tissue in the Waldeyer ring [116]; this occurrence peaks around 6–8 years of age, diminishing then with increasing age.
7. Patients in the pediatric age range may have physiologic linear uptake in epiphyses and apophyses, due to skeletal growth [112].
8. In children, uptake in the salivary glands is variable but typically mild to moderate [116].
9. Endometrial uptake may increase during the ovulatory and menstrual phases in premenopausal females [17].
10. Moderate and diffuse uptake can be seen in the breasts, higher in adolescent girls with dense breasts or in lactating breasts (Fig. 1.15). Also the nipples normally demonstrate activity uptake, better identified in the non-attenuation-corrected images [116, 120].

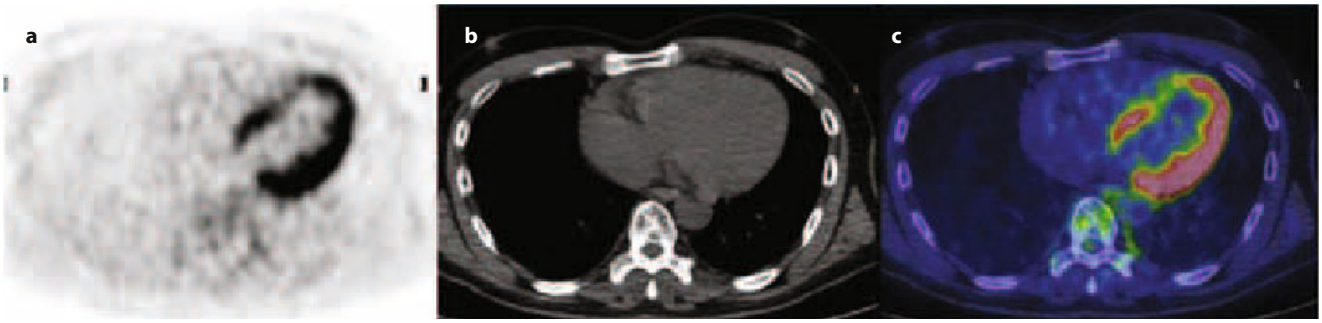

Fig. 1.14 Transaxial [^{18}F]FDG-PET/CT images (PET in **a**, CT in **b**, fused PET/CT in **c**), showing intense myocardial [^{18}F]FDG uptake with an area of reduced uptake in the septum in a patient with left bundle-branch block

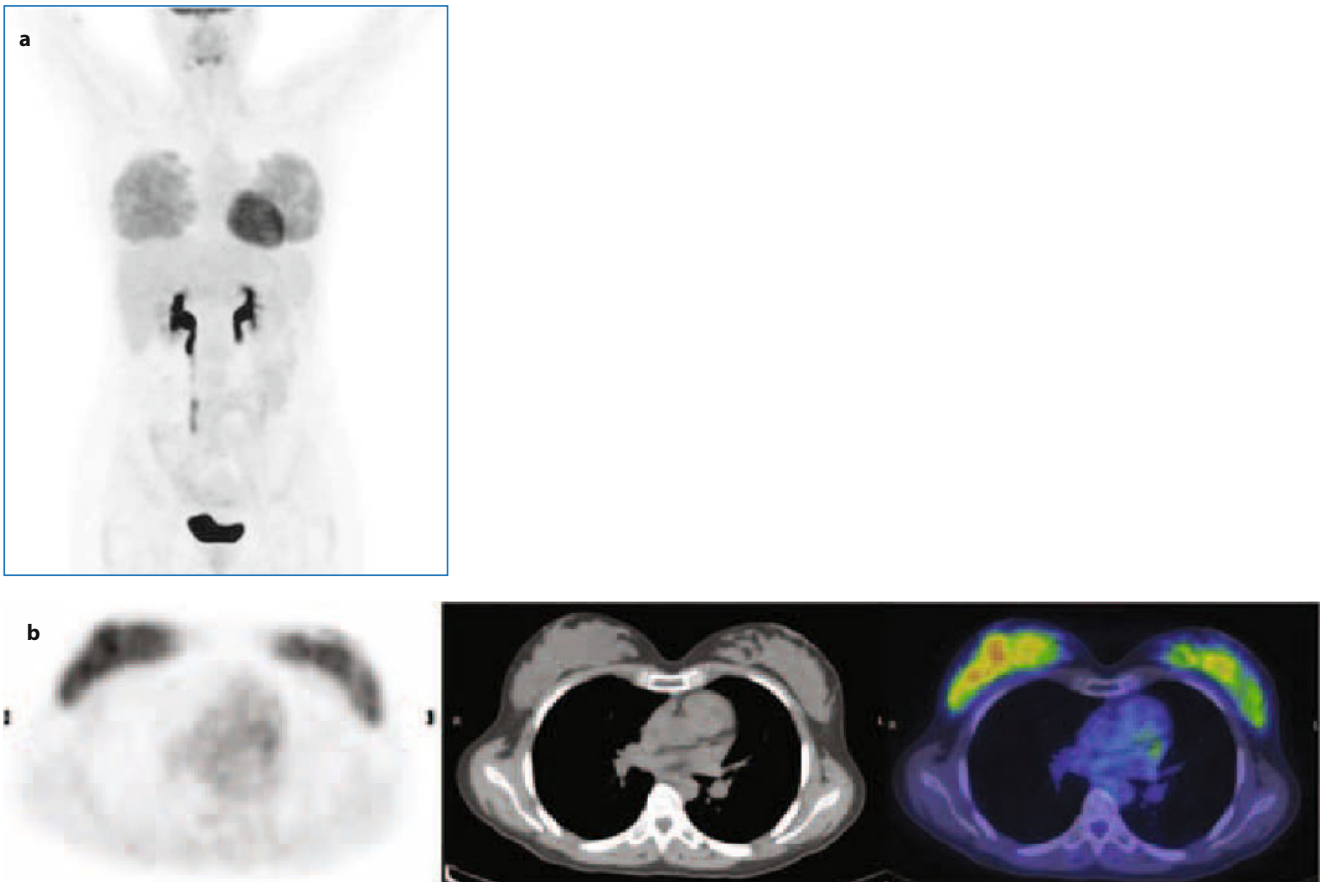

Fig. 1.15 Follow-up [^{18}F]FDG-PET/CT scan in a patient with Hodgkin's lymphoma (complete response lasting for 3 years) who has given birth to a child 2 months earlier. (**a**) MIP image showing intense [^{18}F]FDG uptake in the myocardium as well as in the breasts, with radioactivity accumulation in the renal collecting systems, right ureter and bladder. (**b**) Transaxial [^{18}F]FDG-PET/CT section (PET in *left panel*, CT section in *middle panel*, fused PET/CT in *right panel*), showing intense [^{18}F]FDG uptake at both lactating breasts (more prominent on the right side)

Fig. 1.16 Transaxial [^{18}F]FDG-PET/CT sections (PET in **a**, CT in **b**, fused PET/CT in **c**), showing symmetric and diffuse [^{18}F]FDG uptake at both testicles in an adult patient

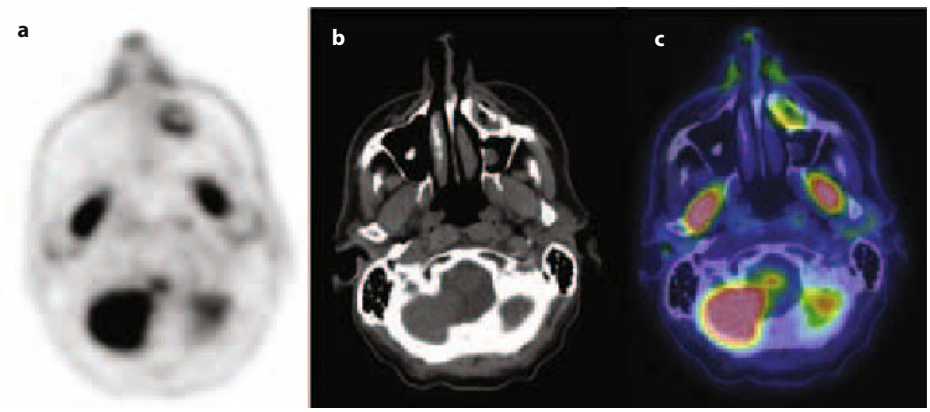

Fig. 1.17 Transaxial [^{18}F]FDG-PET/CT images (PET in a, CT in **b**, fused PET/CT in **c**), showing intense bilateral symmetric [^{18}F]FDG uptake in pterygoid muscles, due to chewing in the period elapsed between tracer injection and acquisition of the scan

Fig. 1.18 MIP of [^{18}F]FDG-PET/CT in a diabetic patient who had received insulin due to hyperglycemia one hour before the examination. Image shows diffuse and inhomogenous radiopharmaceutical uptake in muscles and soft tissues (predominant at right side) resulting in a high background with low brain, liver and kidneys radiotracer localization. Intense radiopharmaceutical uptake is evident at heart and bladder

11. Testicular uptake is usually symmetrical and diffuse, and it may decrease with age [121] (Fig. 1.16).
12. Increased uptake in skeletal muscles (generally symmetric) can occur due to excessive muscle activity during the uptake phase, or within a few hours preceding the PET scan [112] (Fig. 1.17).

1.9.3 Pitfalls

1. Hyperinsulinemia may result in a 'muscle scan' [122] (Fig. 1.18).
2. A well-defined focus of uptake in the lung on ^{18}FDG-PET without a visible corresponding abnormality on the integrated CT (either above or below the diaphragm) can be observed as a consequence of microemboli secondary to paravenous injection. Because the blood clots are admixed with injected radiotracer, they may be very intense [122].
3. Increased bowel uptake can be seen in chronic inflammatory conditions such as enterocolitis and inflammatory bowel disease [17].
4. Markedly increased uptake along the esophagus can occur in patients with esophagitis or after radiation therapy or in patients with hiatal hernia and Barrett esophagus (in the distal esophagus) [112].